Draft version 1.0

ATLAS NOTE

August 25, 2012

Electron Identification Studies for the Level 1 Trigger Upgrade

L. Feremenga[a], M.-A. Pleier[b], F. Lanni[b]

[a]*University of Texas at Arlington*
[b]*Brookhaven National Laboratory*

Abstract

This note shows that it is very difficult to reject neutral pions from electrons at Level 1 trigger of the ATLAS trigger system. The lateral profiles of electrons and neutral pions are different when the interaction point of the colliding protons is at $z = 0$ and a good rejection criteria is achieved. Although this rejection criteria is stable against increasing pileup, it fails for a more realistic model of the luminous profile of the proton beam. A variable used at Level 2 trigger is also shown in this note to be unstable against increasing pileup.

1 Introduction

Throughout its successful operation, the LHC has had a nominal energy increase from $\sqrt{s}$ = 1.8 TeV in 2009 to $\sqrt{s}$ = 7 TeV in 2011 [1][2]. The luminosity has also increased from $2.1 \times 10^{32}\text{cm}^{-2}\text{s}^{-1}$ in 2010 to approximately $7 \times 10^{33}\text{cm}^{-2}\text{s}^{-1}$ in 2012 [3][4]. In 2014, we expect the LHC to collide protons at $\sqrt{s}$ = 13 TeV to 14 TeV after the upgrade [5]. In the following years the LHC will be perfoming precision measurements, in particular on the recently discovered candidate for the Higgs boson. This requires a major upgrade on luminosity because this Higgs candidate has a very low production cross section. By 2019 the LHC is expected to reach an instantaneous luminosity of approximately $3 \times 10^{34}\text{cm}^{-2}\text{s}^{-1}$. This increase in luminosity will impact both the selection efficiency and the trigger rates for low p_{T} objects. An upgrade of the Level 1 trigger was proposed in which groups of cells called *supercells* are used instead of *Trigger Towers* [6].

In this study it is shown that it is not possible to reject neutral pions from electrons using $\Delta\eta \times \Delta\phi = 0.025 \times 0.1$ super-cells. The longitudinal profiles of the electrons and the neutral pions are found to be too similar to be exploited for neutral pions rejection. A variable that relies on the differences between the lateral profiles of neutral pions and electrons to reject neutral pions is introduced. This variable is stable against increasing pileup and separates electrons from neutral pions in the ideal case when the interaction point is at $z = 0$, where it makes optimal use of the projective geometry of the calorimeter. It fails for a more realistic model of the luminous profile of the beam, which is no longer a δ-function at $z = 0$ but a Gaussian distribution with a width of approximately 5 cm. The variable currently used at Level 2 trigger that exploits the two maxima of energy deposited by neutral pions is shown to be less effective against increasing pileup, prompting more detailed studies in the future.

2 The ATLAS Trigger

The ATLAS Trigger system comprises three levels [7][8]. This study is restricted to the first level (L1). At this level, regions in the calorimeter are identified that have energy deposits larger than a predefined threshold. To maintain high processing speeds it is not possible to do this on a cell level and therefore exploit the full granularity of the calorimeter. Coarser regions of size $\Delta\eta \times \Delta\phi = 0.1 \times 0.1$ (Trigger Towers, TT) in the electromagnetic section of the calorimeter (EM Cal) are used instead. The EM Cal has four layers and these are the Presampler (PS) and the first (Layer 1) up to the third layer (Layer 3). Layer 1 comprises strips which are narrower in η than the cells in Layer 2. Layer 2 has the largest radiation length of the EM Cal and therefore receives the largest fraction of energy from electromagnetic objects. Cells in the PS and Layer 2 have the same width in η ($\Delta\eta = 0.025$) and the widest cells in η are in Layer 3 ($\Delta\eta = 0.05$). Figure 1 shows the segmentation of the different layers for the barrel of the calorimeter. In this study we concentrate only on the barrel.

In Layer 2 one TT comprises 4×4 cells in $(\eta \times \phi)$. The current L1 trigger algorithm first runs a sliding window to find a local maximum that comprises 2×2 TTs in (η, ϕ). These 2×2 tower regions shown in green in Figure 2 are called Clusters. The algorithm then computes the horizontal and the vertical sums of energy in this local maximum and labels the highest as the candidate energy for the cluster. It accepts the cluster if this energy is greater than the threshold energy, otherwise the cluster is rejected. The neighboring towers that sorround the cluster make up the Isolation Ring (IR). A ratio of the cluster energy and the IR is a good variable to study the lateral profiles of differenct objects, and in particular can be used to separate EM objects against hadronic objects at trigger level.

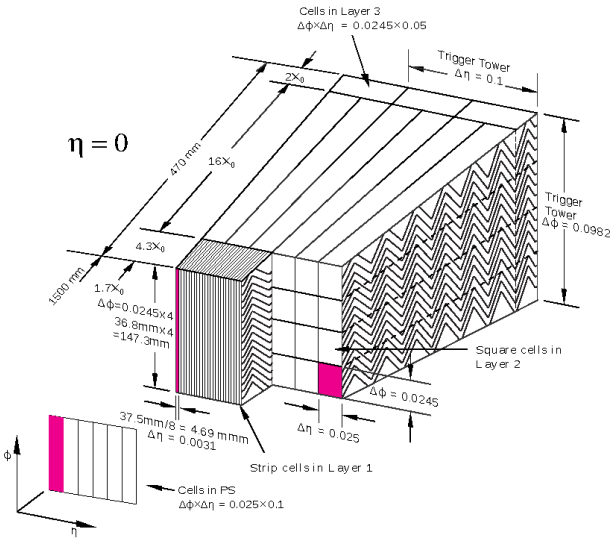

Figure 1: Different layers in the EM Cal. $\eta = 0$ shows that this structure is for the barrel of the calorimeter. End caps have a different layout.

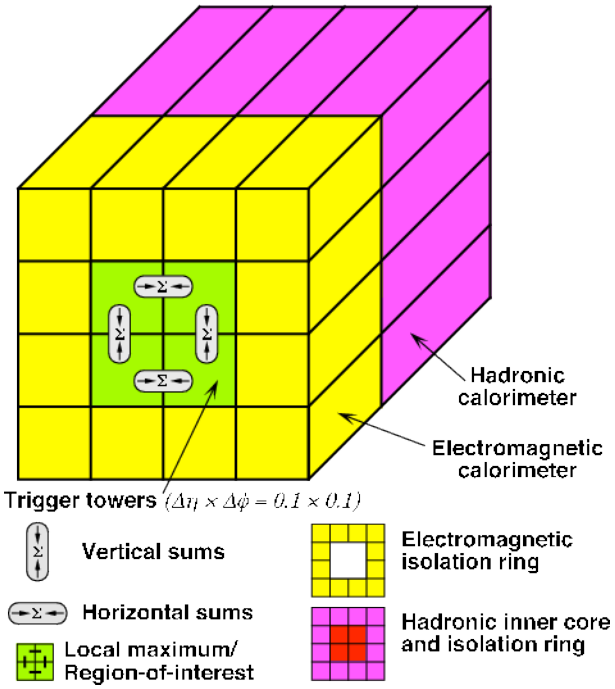

Figure 2: The L1 algorithm for electron-γ identification.

3 Monte Carlo samples

The procedure for obtaining Monte Carlo samples is the following. Single, isolated electrons or neutral pions are generated by an Athena package called ParticleGenerator [9] with a predefined energy and direction in (η, ϕ) in the EM Cal. For simplicity the chosen (η, ϕ) direction (0.4125, 0.1125) is the center of a cell and Geant4 [10] is used to simulate the EM Cal. The output of this simulation is digitized and subsequently reconstructed. D3PDs are made out of the reconstructed data. Figure 3 illustrates the simulation chain used.

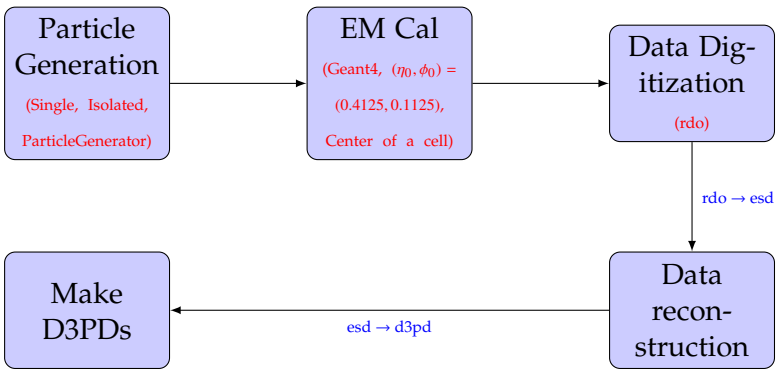

Figure 3: Flowchart of the sample generation chain.

Separate Monte Carlo samples were also made in which electrons and neutral pions were generated over a range in η covering the width of a cell in Layer 2 ($\Delta\eta = 0.025$) which is also the width of a supercell. We will refer to samples generated in this manner as *scanned* η samples. The samples generated as described in the preceding paragraph are *fixed* η samples.

ParticleGenerator by default assumes that the interaction point of the particles in the collider can be described by a $\delta-$function at $z = 0$. This is the ideal situation. A more realistic model describes the interaction point with a Gaussian distribution with RMS $\approx$ 5cm. In this note, we refer to this effect as *Vertex Smearing*.

4 Results

4.1 Longitudinal Profile

One variable ρ_{layer} that quantifies the depth profile of an object is the fraction of energy deposited in a layer of the calorimeter and the total energy deposited in all four layers. In this study, the total energy is the energy deposited in the cluster with the most energy in the barrel of the calorimeter. ρ_{layer} for a particular layer is then the ratio of the energy deposited in the layer and cluster in question, and this total energy:

$$\rho_{layer} = \frac{\sum_{c \in cl, c \in layer}(E_c)}{E_{cl}}, \tag{1}$$

where $layer \in \{0, 1, 2, 3\}$, cl is the cluster that contains the most energy and c represents individual cells whose dimensions depend on the layer. For the PS and for Layer 3 Figure 4 shows that the deposited energy fraction is less than 5% for all studied particle energies. Most of the energy is deposited in Layer 1 and Layer 2. This study therefore concentrates on Layer 1 and Layer 2.

Figure 5 (left) is an overlay of ρ_1 and ρ_2 for both electrons and pions for increasing electron or pion energy. Since we are mostly interested with triggering for low p_T objects, we restrict our analysis to objects with not more than 50 GeV. It is clear from Figure 5 that electrons and pions exhibit similar longitudinal profiles. The plot on the right in the same Figure is a 2-dimensional distribution of ρ_1 vs. ρ_2 for 20 GeV electrons and 20 GeV neutral pions. Both electrons and pions show the expected anticorrelation in ρ_1 and ρ_2; there are no differences strong enough to warrant a separation. Figure 6 shows an example distribution for 20 GeV objects in ρ_1 (left) and for ρ_2 (right). No simple cuts can be made on both variables that will reject a significant fraction of neutral pions without losing more than 5% of electrons.

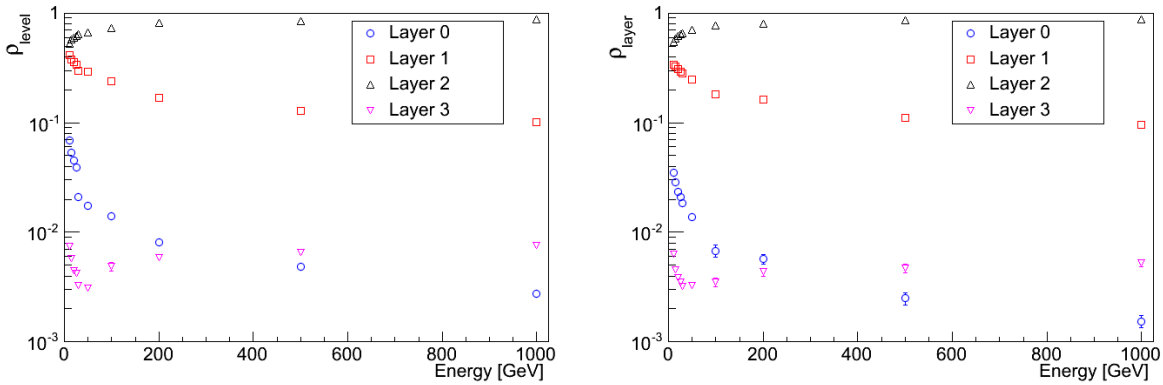

Figure 4: [Left] ρ_{layer} for electrons for all the layers of the EM Cal. [Right] ρ_{layer} for neutral pions for all the layers of the EM Cal.

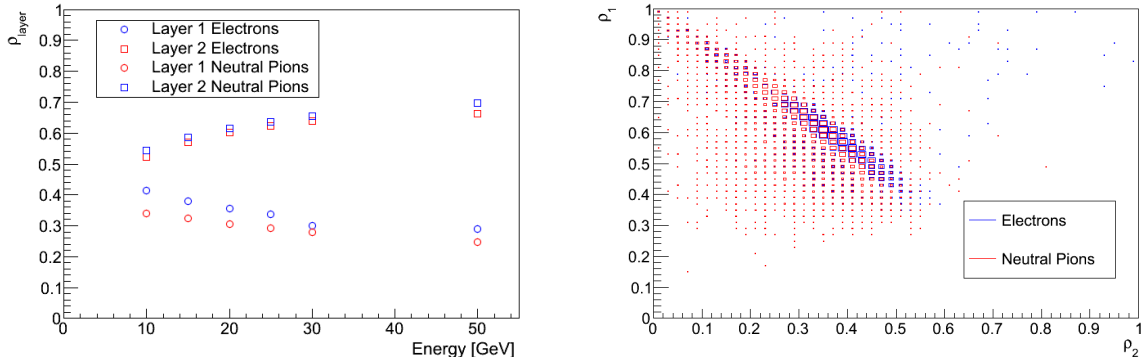

Figure 5: [Left] A comparison of neutral pions and electrons in ρ_1 and ρ_2 versus increasing incident energy. [Right] ρ_1 versus ρ_2 for electrons and neutral pions.

For further comparison between the fraction of energy deposited in Layer 1 and in Layer 2, we introduce

$$\rho_{comp} = \frac{\rho_1}{\rho_2} \tag{2}$$

One advantage that ρ_{comp} has over the other possible variables is that it is less sensitive to pileup because pileup offsets in ρ_1 and in ρ_2 cancel out. That minimizes uncertainties. Figure 7 is an overlay of ρ_{comp} for electrons and neutral pions versus their energy. Again, there are no major differences that can enable separation between these two objects for energies less than 50 GeV.

Figure 8 shows ρ_{comp} for 20 GeV electrons and pions. Again, no simple cuts can be made that will reduce background significantly and yet maintain less than 1% signal loss. Similar studies at different and higher pileups show no differences as expected (Figure 8 right). Pileup therefore does not affect ρ_{comp}. In the next section we will therefore study the possibility of electron-neutral pion separation based on the lateral profiles.

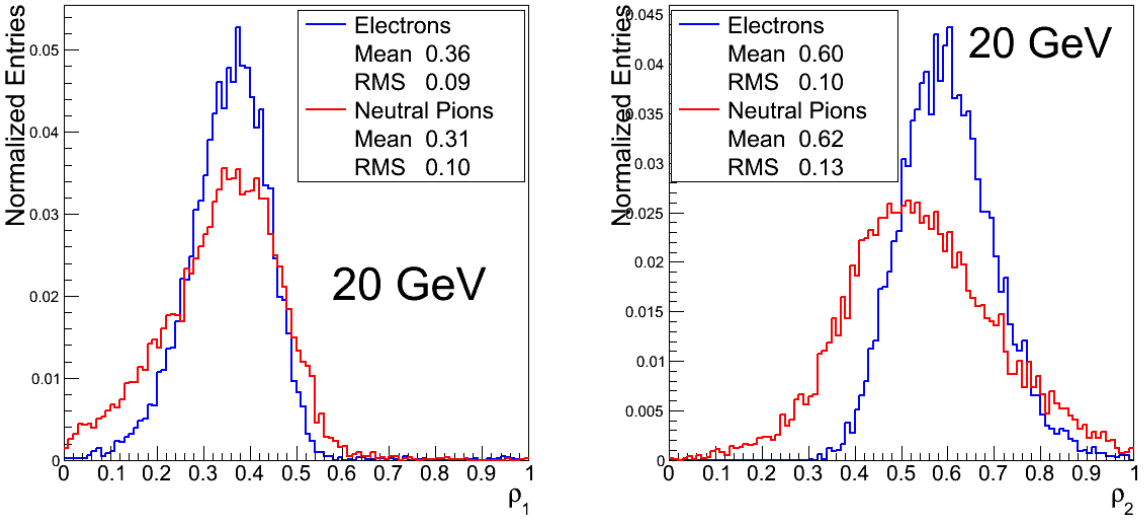

Figure 6: [Left] ρ_1 distribution for 20 GeV electrons and neutral pions. [Right] ρ_2 distribution for 20 GeV electrons and neutral pions.

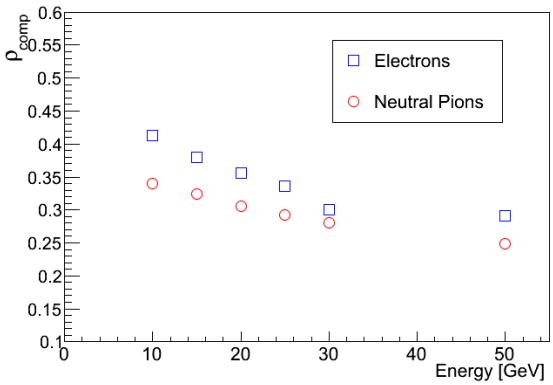

Figure 7: ρ_{comp} versus the incident energy of electrons and neutral pions.

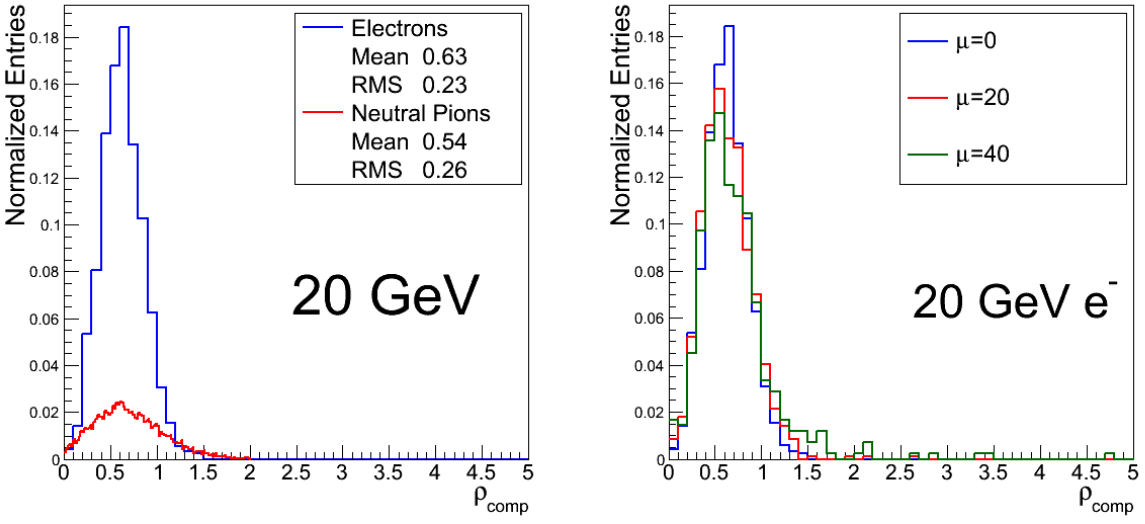

Figure 8: [Left] ρ_{comp} distribution for 20 GeV electrons and neutral pions. [Right] ρ_{comp} distribution for 20 GeV electrons at different pileups.

4.2 Lateral Profile

The electron-γ identification algorithms used offline and those used for the Level 2 trigger have access to full granularity. Offline algorithms are used as a benchmark for any differences between the lateral profiles of the electrons and the neutral pions. These differences can therefore offer some insight onto rejection techniques for triggering. In Layer 1, one variable that quantifies this is the number of strips that have both energy hits above a certain threshold and the same ϕ position as the strip with the most energy. Figure 9 (left) shows this variable versus the energy of electrons and neutral pions. The threshold energy here is 1% of the energy contained in the cluster with the most energy. For low energy objects, and hence for low p_{T} objects, a separation between electrons and neutral pions can be easily deduced since for objects with energy less than 30 GeV the profile for neutral pions is on average one strip wider. Figure 9 (right) shows an example distribution for 20 GeV objects. Since in Layer 1 the supercells are 8 strips wide (Figure 1), we can deduce from Figure 9 (right) that the energy shower in Layer 1 is contained in at most two neighboring supercells for the no-pileup case ($\mu = 0$). For 20 GeV electrons Figure 10 shows that at higher pileup the electron profile does not change [1]. This implies that neutral pions at higher pileup also have a wider energy shower.

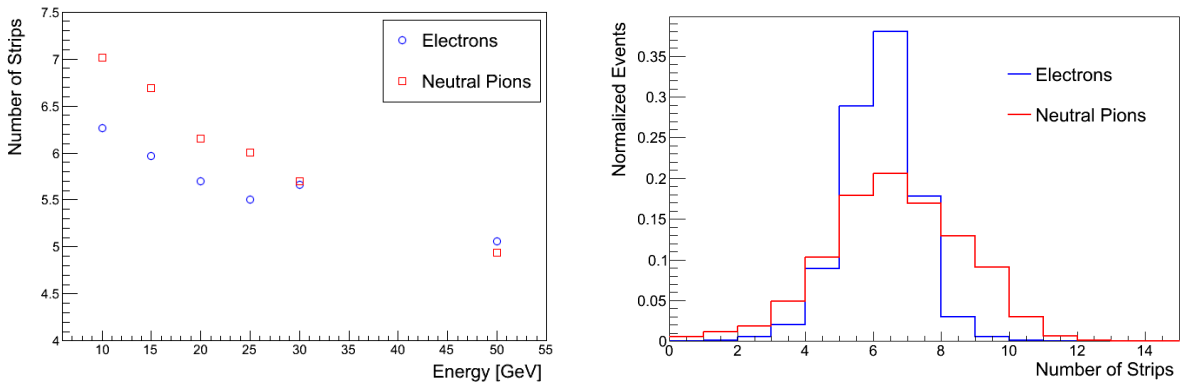

Figure 9: [left] Mean number of strips with hits > 1% of cluster energy vs. e^-/π^0 energy. [right] Mean number of strips with hits > 1% of cluster energy at 20GeV for electrons and neutral pions

4.2.1 $R_\eta^{(1)}$

For online neutral pion rejection we introduce

$$R_\eta^{(1)} = \frac{E_0}{E_1 + E_0 + E_{-1}} \tag{3}$$

where E_0 is the energy deposited in the supercell with the most energy and $E_{\pm l}$ is the energy deposited in $\pm l$ supercells around the supercell in η with the most energy. We use three supercells here since the energy shower is contained in at most two supercells (Figure 9 (right)). The left plot in Figure 11 shows how $R_\eta^{(1)}$ for electrons differs from that of neutral pions for increasing energies and the one on the right in the same Figure shows the distribution for 20 GeV electrons and neutral pions as an example. Distributions shown in Figure 11 are from Monte

[1] The Monte-Carlo samples used for electrons in Figure 9 (right) are not the same as those used for $\mu = 0$ in Figure 10. This explains why the distributions are not identical.

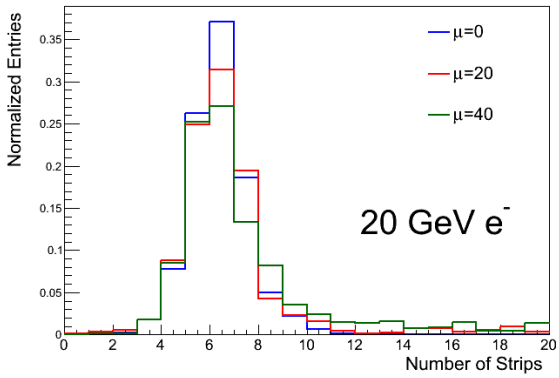

Figure 10: Number of strips with hits > 1% of cluster energy at different pileups, for 20 GeV electrons

Carlo samples with vertex smearing turned off and fixed η. For low p_{T} objects, a good separation can be achieved between electrons and neutral pions. For 20 GeV objects when vertex smearing is turned off, a rejection criteria based on $R_{\eta}^{(1)}$ can reject more than 50% of neutral pions while losing less than 5% of the total electrons.

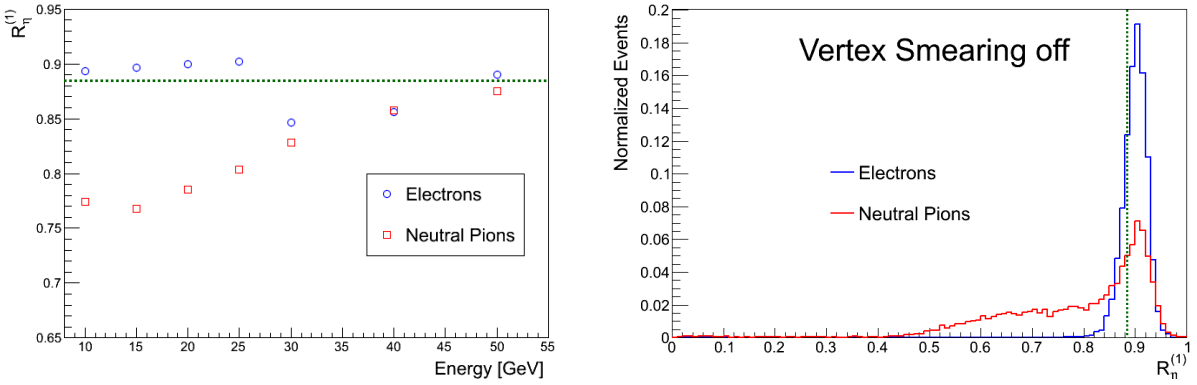

Figure 11: [Left] $R_{\eta}^{(1)}$ versus the incident energy of electrons and neutral pions when vertex smearing is turned off and fixed η. [Right] $R_{\eta}^{(1)}$ for 20 GeV electrons and neutral pions when vertex smearing is off and η is fixed.

Figure 12 shows how the distribution for $R_{\eta}^{(1)}$ changes for 20 GeV electrons and neutral pions when vertex smearing is turned on. When vertex smearing is turned on, projection onto a single supercell deteriorates for a fraction of events. This is evident from a tail that develops for the electron $R_{\eta}^{(1)}$ distribution. The change in the tail is not apparent for neutral pions because their distribution is spread out even without vertex smearing. The result of this is a loss of separation between electrons and neutral pions when vertex smearing is turned on. Since the the model with vertex smearing is more realistic, we restrict our analysis to that.

Figure 13 shows $R_{\eta}^{(1)}$ when electrons or neutral pions are scanned over a $\Delta\eta = 0.025$ range, which is the width of a supercell in η. As expected, scanning over η does not restore the separation between electrons and neutral pions. There are also no major differences between scanning and fixing η, so restrict our studies to the case when η is fixed.

The algorithm that calculates $R_{\eta}^{(1)}$ first identifies the supercell with the highest energy in Layer 2 and then uses the same (η, ϕ) position to identify the supercell with the highest energy

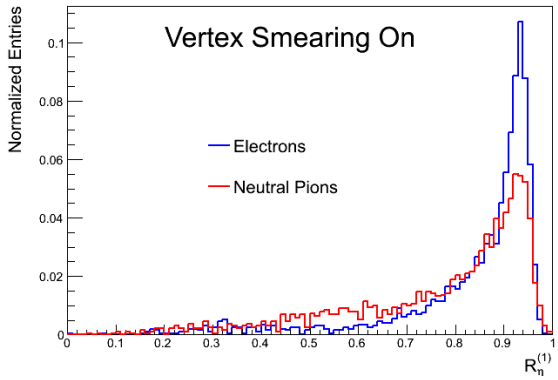

Figure 12: $R_\eta^{(1)}$ for 20 GeV electrons and neutral pions when vertex smearing is on and η is fixed.

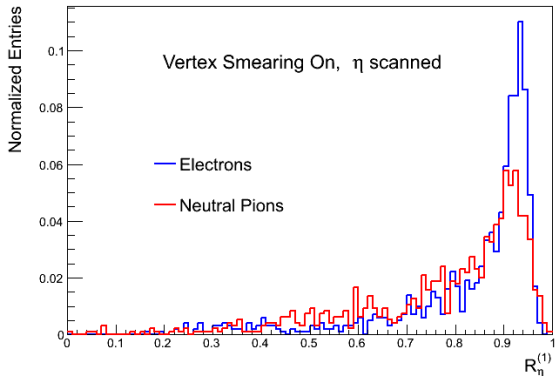

Figure 13: $R_\eta^{(1)}$ for 20 GeV electrons and neutral pions when vertex smearing is on and η is scanned.

in Layer 1. This approach correctly identifies the supercell with the highest energy in Layer 1 when vertex smearing is turned off, but when the vertex smearing is turned on it is possible to wrongly identify this supercell. Rather than using collider coordinates (η, ϕ) to identify cells and supercells, we label each cell and supercell with two individual indices $(i\eta, i\phi)$. The variable

$$\Delta\eta = i\eta_{H1} - i\eta_{H2}, \tag{4}$$

quantifies how aligned the supercells are in Layer 1 and Layer 2, where $i\eta_{Hj}$[2] is the η index for the supercell in layer j with the highest energy. The left plot in Figure 14 shows how $\Delta\eta$ changes when vertex smearing is on. When vertex smearing is off, using the supercell in layer 2 as the seed correctly identifies the highest-energy supercell in layer 1. When vertex smearing is turned on, this algorithm fails for a fraction of events so it becomes important to seed from Layer 1. The right plot in Figure 14 shows $R_\eta^{(1)}$ when the highest-energy supercell is seeded from Layer 1, and when vertex smearing is turned on. Since almost all the energy is deposited in two neighboring supercells, the highest-energy one included, when the correct supercell is identified $R_\eta^{(1)}$ is always greater than or equal to 0.5. The fraction of events that a supercell is incorrectly identified when seeding from Layer 2 is so small that correcting the seed does not yield a visible improvement in separation between electrons and neutral pions.

[2]This index is weighted with energy. $i\eta_{Hj} = \frac{\sum_k E_k \times i\eta_k}{\sum_k E_k}$ where $k \in \{0, \pm 1\}$ identifies the supercells, 0 being the highest-energy supercells and ±1 is for the neighboring supercells.

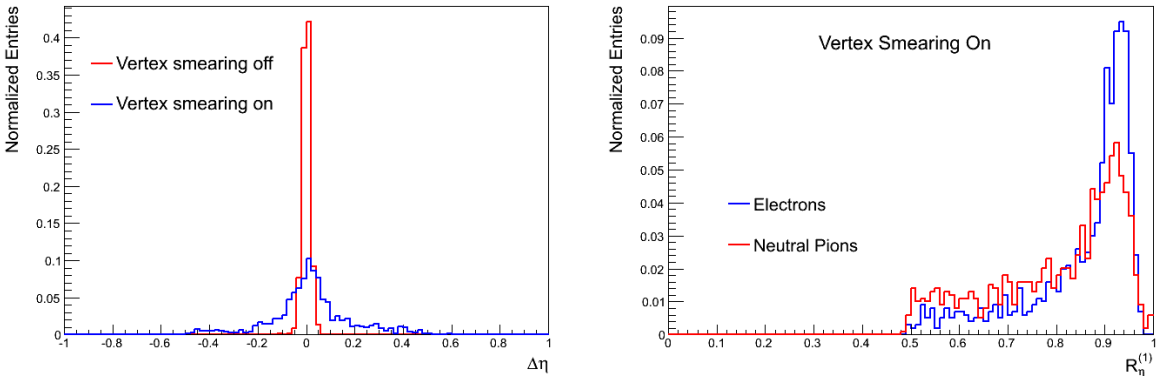

Figure 14: [Left] $\Delta\eta$ for electrons when vertex smearing is turned on and off. [Right] $R_\eta^{(1)}$ when seeding the highest-energy supercell from Layer 1 instead of Layer 2. Vertex smearing is also turned on.

4.2.2 E_r for Level 2

Although the energy deposit from neutral pions is often found to have two maxima because of the $\pi^0 \rightarrow \gamma\gamma$ decay, these two maxima are normally within one supercell in η. It is therefore not possible to exploit this property to separate them from electrons at Level 1 trigger using supercells. At Level 2 the variable

$$E_r = \frac{E_{max} - E_{smax}}{E_{max} + E_{smax}} \tag{5}$$

is used, where E_{max} is the energy deposited in the strip that receives the most energy and E_{smax} is the energy deposited in the strip that receives the second largest energy deposit. Since electrons normally have one maximum of energy deposition, E_r is expected to be close to 1; for neutral pions the distribution is expected to be more spread out. Figure 15 shows a good separation achieved at level 2 trigger using this variable. The plot on the right in Figure 15 shows that E_r is stable after turning vertex smearing on. This shows that at full granularity, it is possible to separate electrons from neutral pions at Level 2 trigger. Figure 16 shows that E_r is also stable after introducing scanning. As pointed out before, there are no major differences between scanning over η and not scanning over η.

Figure 17 shows the electron efficiency when E_r is used at Level 2 trigger and when $R_\eta^{(1)}$ is used at Level 1. E_r is stable against vertex smearing. At Level 2 E_r can reject 60% neutral pions while losing not more than 2% electrons (top left). When vertex smearing is turned on, 60% neutral pions can also be rejected while losing not more than 2% even when η is scanned (bottom left). $R_\eta^{(1)}$ deteriorates when vertex smearing is turned on (top right). The deterioration of $R_\eta^{(1)}$ is consistent also when η is scanned (bottom right).

Figure 18 shows the electron efficiency when E_r is used at different pileups. It is clear that rejection of neutral pions from electrons is significantly reduced at higher pileups when using E_r. This warrants further investigation in future studies.

5 Summary and Conclusions

In order to keep exploring new physics at the LHC using the ATLAS detector we need to upgrade its trigger system so that it can accomodate low p_{T} objects that come from rare events. Increasing the granularity of trigger from Trigger Towers to supercells is one of the ways that the

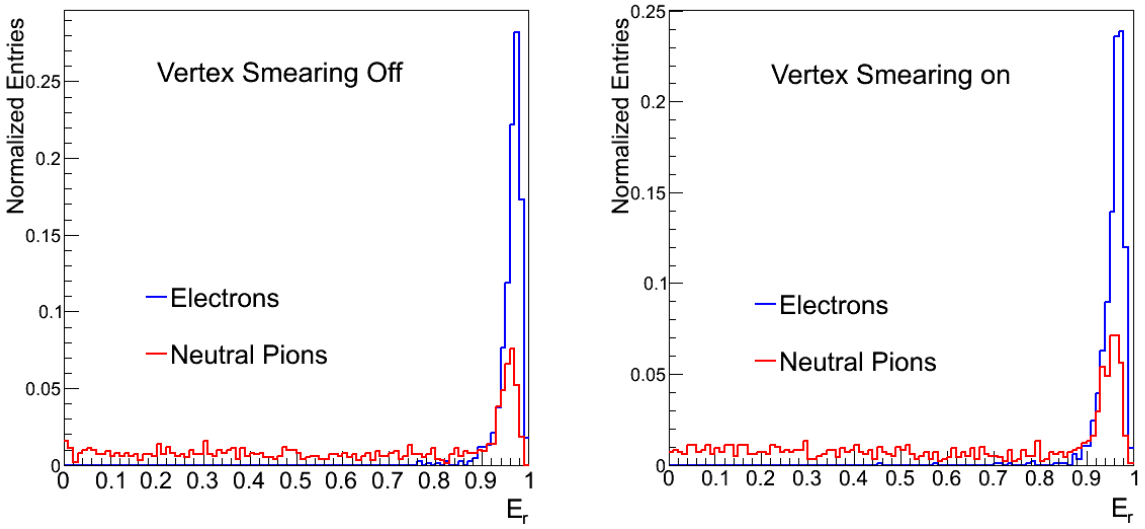

Figure 15: [Left] E_r when vertex smearing is turned off. [Right] E_r when vertex smearing is turned on.

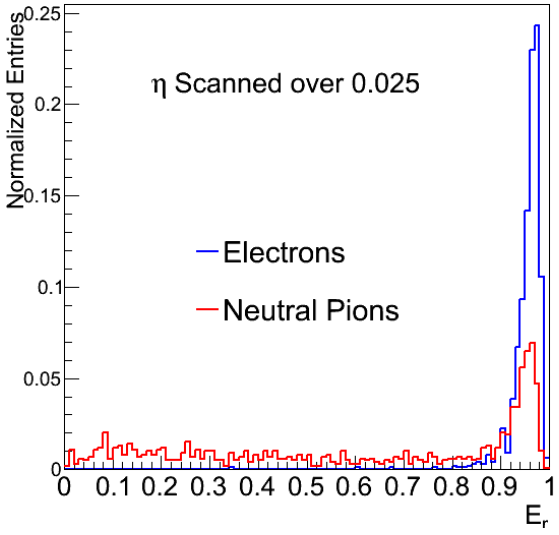

Figure 16: E_r is not affected by scanning. Good separation between electrons and neutral pions is achieved both when η is fixed and when it is scanned over a range.

Level 1 trigger can be improved. Using supercells in Layer 1 of the electromagnetic calorimeter however does not achieve a separation of electrons from neutral pions. In the ideal case when the interaction point of the colliding protons is at $z = 0$ $R_{\eta}^{(1)}$ can achieve a good separation between electrons and neutral pions. In a more realistic case when the luminous profile of the colliding beams is more spread out this separation is greatly reduced. Although the variable E_r, used at Level 2 trigger to reject neutral pions from electrons is stable against spreading out the luminous profile of the beam, it becomes inefficient as pileup increases and will likely be unusable in Phase-I upgrade conditions ($\mu = 80$) and beyond. Futher studies therefore have to be done to improve not only the Level 1 trigger of ATLAS but also the Level 2 trigger.

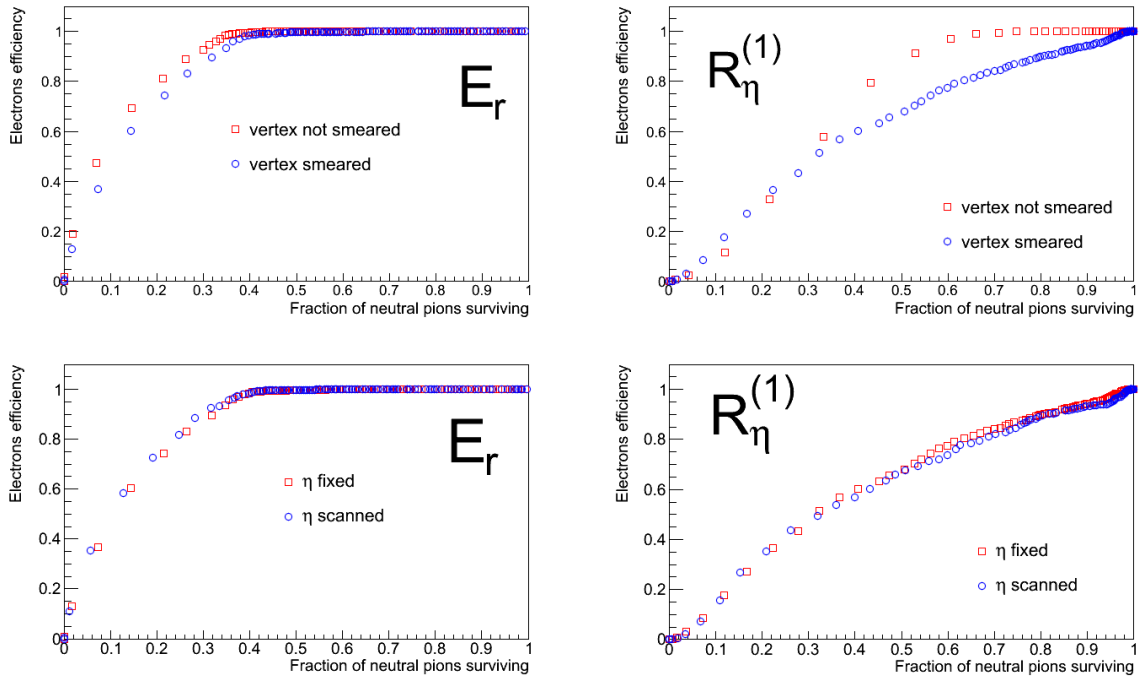

Figure 17: [Top Left] Electron efficiency versus the fractions of neutral pions surviving using E_r with and without vertex smearing. [Top Right] Electron efficiency versus the fraction of neutral pions surviving using $R_\eta^{(1)}$ with and without vertex smearing. [Bottom Left] Electron efficiency versus the fractions of neutral pions surviving using E_r with fixed and scanned η, when vertex smearing is turned on. [Bottom Right] Electron efficiency versus the fractions of neutral pions surviving using $R_\eta^{(1)}$ with fixed and scanned η, when vertex smearing is turned on.

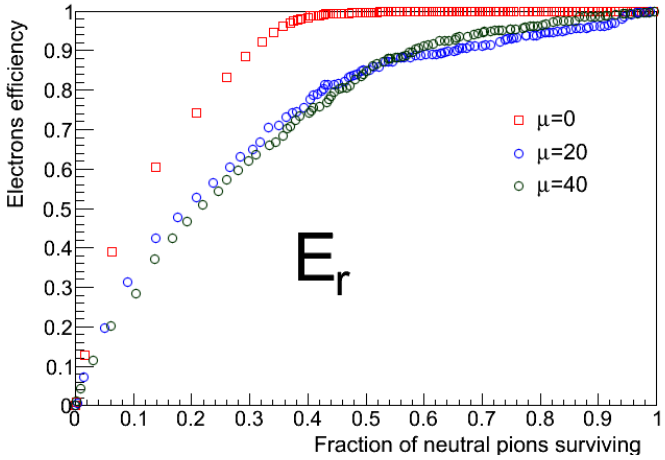

Figure 18: E_r becomes ineffective at high pileups.

6 Acknowledgements

We would like to thank Hong Ma for the hours he spent helping us work in the Athena framework. Also, we are thankful to Jaehoon Yu for the consistent conversations that gave some

insight onto the direction that this study took.

References

[1] ALICE Collaboration, K. Aamodt et al., *First proton-proton collisions at the LHC as observed with the ALICE detector: Measurement of the charged particle pseudorapidity density at s**(1/2) = 900-GeV*, Eur.Phys.J. **C65** (2010) 111–125, arXiv:0911.5430 [hep-ex].

[2] ATLAS Collaboration, *Further search for supersymmetry at sqrt(s) = 7 TeV in final states with jets, missing transverse momentum and isolated leptons with the ATLAS detector*, arXiv:1208.4688 [hep-ex].

[3] ATLAS Collaboration, *Peak stable luminosity recorded at the end of 2010*, 2010. https://atlas.web.cern.ch/Atlas/GROUPS/DATAPREPARATION/DataSummary/2010/daily-summary.html.

[4] ATLAS Collaboration, *Peak stable luminosity recorded at the end of 2012*, 2012. https://atlas.web.cern.ch/Atlas/GROUPS/DATAPREPARATION/DataSummary/2012/.

[5] *Letter of Intent for the Phase-I Upgrade of the ATLAS Experiment*, Tech. Rep. CERN-LHCC-2011-012. LHCC-I-020, CERN, Geneva, Nov, 2011.

[6] D. O. Damazio and F. Lanni, *Higher electromagnetic calorimeter segmentation to improve trigger selectivity in high luminosity scenarios*, Tech. Rep. ATL-LARG-INT-2012-002, CERN, Geneva, Mar, 2012.

[7] *ATLAS detector and physics performance: Technical Design Report, 1*. Technical Design Report ATLAS. CERN, Geneva, 1999. Electronic version not available.

[8] *ATLAS detector and physics performance: Technical Design Report, 2*. Technical Design Report ATLAS. CERN, Geneva, 1999. Electronic version not available.

[9] ATLAS Collaboration, W. Seligman, *ParticleGenerator, A Simple Monte-Carlo Generator for Athena*, 2005. http://atlas-sw.cern.ch/cgi-bin/viewcvs-atlas.cgi/offline/Generators/ParticleGenerator/doc/ParticleGenerator.pdf?view=co.

[10] Geant4 Collaboration, *Geant4*, 2012. http://geant4.cern.ch/.